International Journal of Nanomedicine

Dovepress
open access to scientific and medical research

Open Access Full Text Article

ORIGINAL RESEARCH

Polydopamine-Based Targeted Nanosystem for Chemo/Photothermal Therapy of Retinoblastoma in a Mouse Orthotopic Model

Bo Jin[1], Kexin Lu[2], Wenna Gao[1], Yixian Liu[3], Mengfei Wang[2], Xiaojun Zhang[3], Huiping Chen[3], Liyun Zheng[3], Min Zou[3]

[1]Department of Ophthalmology, the First Affiliated Hospital of Zhengzhou University, Zhengzhou University, Zhengzhou, Hennan, 450052, People's Republic of China; [2]BGI College, Zhengzhou University, Zhengzhou, 450052, People's Republic of China; [3]Henan Institute of Medical and Pharmaceutical Sciences, Zhengzhou University, Zhengzhou, 450052, People's Republic of China

Correspondence: Min Zou; Liyun Zheng, Email Minzou1980@126.com; zhengliyun@zzu.edu.cn

Background: At present, the few photothermal/chemotherapy studies about retinoblastoma that have been reported are mainly restricted to ectopic models involving subcutaneous implantation. However, eyeball is unique physiological structure, the blood-retina barrier (BRB) hinders the absorption of drug molecules through the systemic route. Moreover, the abundant blood circulation in the fundus accelerates drug metabolism. To uphold the required drug concentration, patients must undergo frequent chemotherapy sessions.

Purpose: To address these challenges above, we need to develop a secure and effective drug delivery system (FA-PEG-PDA-DOX) for the fundus.

Methods: We offered superior therapeutic efficacy with minimal or no side effects and successfully established orthotopic mouse models. We evaluated cellular uptake performance and targeting efficiency of FA-PEG-PDA-DOX nanosystem and assessed its synergistic antitumor effects in vitro and vivo. Biodistribution assessments were performed to determine the retention time and targeting efficiency of the NPs in vivo. Additionally, safety assessments were conducted.

Results: Cell endocytosis rates of the FA-PEG-PDA-DOX+Laser group became 5.23 times that of the DOX group and 2.28 times that of FA-PEG-PDA-DOX group without irradiation. The fluorescence signal of FA-PEG-PDA-DOX persisted for more than 120 hours at the tumor site. The number of tumor cells (17.2%) in the proliferative cycle decreased by 61.6% in the photothermal-chemotherapy group, in contrast to that of the saline control group (78.8%). FA-PEG-PDA-DOX nanoparticles(NPs) exhibited favorable biosafety and high biocompatibility.

Conclusion: The dual functional targeted nanosystem, with the effects of DOX and mild-temperature elevation by irradiation, resulted in precise chemo/photothermal therapy in nude mice model.

Keywords: retinoblastoma, orthotopic model, nanoparticle, synergistic therapy

Introduction

Retinoblastoma (RB) is a malignant intraocular tumor typically found in early childhood, accounting for approximately 4% of childhood cancers.[1] Previous research indicates that RB is attributed to mutations or biallelic loss of the retinoblastoma suppressor gene (RB1).[1,2] If the medical treatment at an early stage proves ineffective, the consequences may include vision loss or metastasis, particularly in the central nervous system (CNS).[3] In underdeveloped countries, the mortality rate for children with RB ranges from 50 to 70%.[4,5] There remains a gap in meeting the needs for innovation and validation of therapeutic methods. Currently, local drug delivery of RB can be achieved through either intra-arterial chemotherapy (IAC) or direct intravitreal administration of chemotherapeutic drugs. However, the operation of IAC implementation[6] is intricate and comes with a high cost. Furthermore, multiple interventional artery treatments may carry the risk of serious complications. Direct intravitreal injection presents potential adverse side effects, particularly with frequent injections.[2] Consequently, there is a need to explore local non-invasion modalities for treating RB, which can offer superior therapeutic efficacy with minimal

Received: 8 March 2024
Accepted: 21 July 2024
Published: 30 July 2024

or no side effects. Photothermal therapy (PTT) commonly employs near-infrared (NIR) light-absorbing agents to induce hyperthermia, leading to tumor cell apoptosis. This technique possesses several advantages, including low invasiveness, high therapeutic specificity for destroying tumor cells, and relatively low biological toxicity.[7] In comparison to ultraviolet (UV) or visible (Vis) light, NIR light has greater tissue penetration capabilities. Consequently, the deep tissue penetration of NIR light can be harnessed to treat various cancers.[8,9] Numerous studies have explored PTT in inhibiting tumors, including breast, brain, and prostate.[10–12] Cancer cells can get repaired with the help of heat shock proteins (HSPs) under hyperthermia, resulting in reduced treatment efficiency and therapeutic resistance.[13] In addition, enormous volumes of reactive oxygen species (ROS) are generated due to the hyperthermia, they trigger an adverse inflammatory response, impeding the efficacy of the treatment.[8]

To achieve a better therapeutic effect, researcher have proposed that mild-temperature PTT is highly desirable strategy,[13] or combined with other modes of treatment, such as chemotherapy.[14,15]

However, the few photothermal/chemotherapy studies that have been reported are mainly restricted to ectopic models involving subcutaneous implantation.[3,16–18] Orthotopic models, which closely mimic the biological characteristics of clinical tumors, are rarely featured in research to date. The primary distinction between subcutaneous and orthotopic animal models lies in the tumor microenvironment, impacting the tumor immune response and treatment outcomes. The eyeball is unique physiological structure, BRB serves as a primary obstacle to the ocular absorption of molecules through the systemic route.[19] Furthermore, the fundus experiences a high intensity of blood circulation, accelerating drug metabolism.[20,21] To sustain the necessary drug concentration, patients must undergo frequent chemotherapy sessions with high doses. Delivering adequate photosensitive materials and drugs to RB tumor cells remains a crucial aspect of photothermal-chemotherapy for treating retinoblastoma.

In this study, we addressed these challenges and developed a carrier based on polydopamine (PDA) linked to a folic acid (FA) ligand through the PEG bridge (Scheme 1A). Subsequently, we loaded doxorubicin (DOX) to create the positively

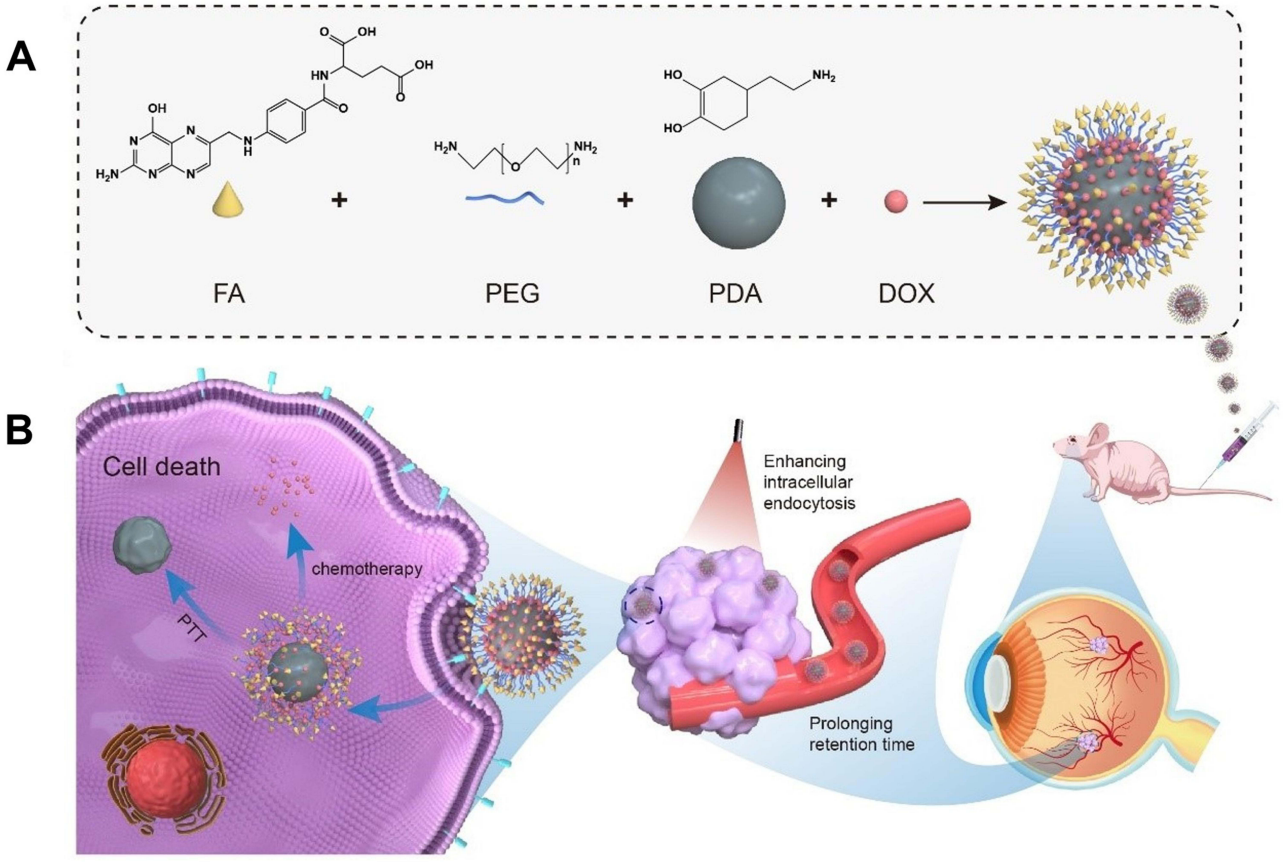

Scheme 1 Schematic of (**A**) the synthesis of FA-PEG-PDA-DOX NPs and (**B**) underlying mechanisms of the synergistic photothermal and chemical therapy for Y79 retinoblastoma. FA-PEG-PDA-DOX consisted of four components, which were folate ligand (FA), polyethylene glycol (PEG), Polydopamine (PDA) and chemotherapeutic agent: doxorubicin (DOX).

charged drug delivery system (FA-PEG-PDA-DOX) (around 99nm), as illustrated in Scheme 1A. In vitro, we evaluated the developed system's cellular uptake performance and targeting efficiency and assessed its antitumor effects and photothermal conversion efficacy. In vivo assessment included the evaluation of photothermal conversion and the synergistic antitumor efficacy of the FA-PEG-PDA-DOX NPs. Safety assessments were conducted to estimate their toxicity on major target organs. Additionally, the retention time and targeting efficiency of the NPs were determined by biodistribution assessments in vivo.

As depicted in Scheme 1B, the operational procedure of this system was divided into four steps: (i) Following administering through tail vein injection, the PEG fragment of nanoparticles served as a protective layer, rendering the drug less accessible for clearance by the immune system, thereby improving the blood circulation time in vivo. (ii) The targeting FA ligand guided the NPs to specifically bind to folate receptors (FRs), which are specific markers on the surface of Rb cells.[16,17,22] The nanosized particles and morphology of the NPs concurrently mediate the process of phagocytosis, due to the enhanced permeability and retention (EPR) of nanomedicine.[23,24] (iii) Photothermal conversion facilitates the endosomal escape of nanodrugs, realizing synergistic effects. (iv)In the acidic tumor microenvironment, PDA can gradually disintegrate and release the loaded drugs.[25]

Materials and Methods

Materials

Ammonia (aqueous), dopamine hydrochloride, doxorubicin (DOX), FA-PEG-NH2, and phosphate buffer saline (PBS) were purchased from Aladdin Technology (Shanghai, China). 1.1′-dioctadecyl-3,3,3′,3′- tetramethylindocarbocyanine perchlorate (DiI), 3.3'-dioctadecyloxacarbocyanine perchlorate (DiO), Roswell Park Memorial Institute-1640 (RPMI-1640), and 2-(4-amidinophenyl)-6-indolecarbamidine dihydrochloride (DAPI) were obtained from Beyotime Biotechnology(China).1,1-dioctadecyl-3,3,3,3-tetramethylindotricarbocyanine iodide (DiR) was received from Abbkine (China). Fetal bovine serum (FBS) was obtained from Capricorn Scientific GmbH (Ebsdorfergrund, Germany). The cell counting kit-8 (CCK-8) assay was obtained from Dojindo Laboratories (Kumamoto, Japan).

Synthesis of PDA

An aqueous ammonia solution (0.5 mL, NH_4OH, 28–30%) and ethanol (20 mL) were mixed in deionized water (45 mL) with stirring at 25 °C. Subsequently, using a syringe, dopamine hydrochloride (180 mg) was added in deionized water (5 mL) and slowly dissolved to the obtained mixture. The color of this solution immediately turned to pale, and gradually changed to dark brown. The reaction solution was stirred for 24 h. PDA NPs were obtained by centrifugation (4000 rpm, 3 min) and washed with deionized water using an ultrafiltration centrifuge tube (3 kd) three times.[26,27]

Synthesis of FA-PEG-PDA

FA-PEG-NH_2 (28 mg) and PDA (10 mg) in 3 mL deionized water were sonicated for 3 min to disperse. The mixture was then stirred away from light, at 300 rpm for 2 h. Then, the solution was centrifuged, removed the the water, then, FA-PEG-PDA NPs were obtained and washed three times. FA-PEG-PDA was sonicated, redispersed in deionized water, and stored at 4 °C for subsequent experiments.[26,28]

Preparation of FA-PEG-PDA-DOX

Doxorubicin (3.2 mg) was accurately weighed, dissolved with PBS, and stirred for 0.5 h. It was then added to the FA-PEG-PDA solution, and the reaction continued for another 4 h away from light at room temperature. The resulting solution was centrifuged at a high speed (12000 rpm, 3 min), washed with deionized water, and redispersed in deionized water, before being stored at 4 °C.[29]

Dynamic Light Scattering (DLS)

The zeta potential and distribution of FA-PEG-PDA nanoparticles were assessed using dynamic light scattering (DLS) with a Nano ZS90 instrument from (Malvern Instruments, UK). All solutions were prepared by adding deionized water under vortexing conditions. The reported values represent the averages of three measurements for each sample.

Transmission Electron Microscopy (TEM)

Morphology images were captured using Tecnai 12 transmission electron microscopy (FEI, America). For each sample, 10 μL of the dispersed solution was dropped onto a copper grid. After drying, the morphologies of the nanoparticles were observed under TEM and photographed.

UV-Vis Absorption Spectrum

The UV-vis absorption spectrum of nanoparticles was measured using a Lambda 35 spectrophotometer (PerkinElmer, USA). The dispersed solution (10 mg/mL) were prepared by adding deionized water under vortexing conditions. An average value was obtained from three measurements for each sample at 25 ◦C.

Stability of FA-PEG-PDA-DOX NPs

To investigate the stability of FA-PEG-PDA-DOX NPs, FA-PEG-PDA-DOX NPs were dispersed in PBS and DMEM medium using an ultrasonic bath at room temperature during three weeks.

Drug Loading

Drug loading was obtained using high-performance liquid chromatography (HPLC). Standard solutions with various concentrations were prepared, and the peak area of the standard liquid at 480 nm was detected using HPLC. The mobile phase consisted of methanol, acetonitrile, glacial acetic acid, and ammonium phosphate dibasic (v/v, 50:10:0.5:40). The chromatographic column was a Diamonsil C18 (5 μm, 250×4.6 mm), and the standard curve was established by plotting the peak area A against the corresponding concentration C.The encapsulation efficiency (EE) and drug loading (DL) content and was calculated:

$$\mathrm{EE}\,(\%) = (\text{amount of initial DOX} - \text{amount of residual DOX}/\text{the amount of initial DOX}) \times 100\%$$

$$\mathrm{DL}\,(\%) = (\text{amount of initial DOX} - \text{amount of residual DOX}/\text{amount of nanoparticles}) \times 100\%$$

In vitro Investigation of Drug Release profiles

The drug release from FA-PEG-PDA-DOX and FA-PEG-PDA-DOX + laser group under different pH conditions was assessed using dialysis. Precise amounts of FA-PEG-PDA-DOX were weighed and dissolved in 1 mL buffers solution at pH 5.0 and PBS at pH 7.4. This resulted in a final concentration of DOX in 0.5 mM solution. The sample was dialyzed by a membrane with a molecular weight cutoff (MWCO of 8000 kda) at 37 °C constant temperature shaker, and 20 mL of buffer fluid served as the release medium. In the FA-PEG-PDA-DOX NPs + laser group, NIR irradiation was applied, raising the temperature to 45 ° C. Subsequently, the sample was transferred to a constant temperature shaker set at 45 °C. Then, 200 μL of the test solution was taken at 1 h, 2 h, 4 h, 8 h, 12 h, 24 h, 48 h and 72 h respectively. Fresh PBS was added to the residual solution to restore the original volume. The 200 μL liquid to be tested underwent centrifugation (10000 rpm, 5 min), and precisely 20 μL was extracted for sample analysis.[30]

Evaluation of in vitro Photothermal Conversion Efficiency

The temperature alteration resulted from the NIR laser exposure to the PDA and FA-PEG-PDA-DOX standard solution. The prepared solution was exposed to an 808 nm near-infrared laser (MDL-III-808, Changchun New Industries Optoelectronics Technology Co., Ltd.) at room temperature for 5 min, positioned 5 cm away from the sample, with an irradiation power density of 1 W/cm2. Deionized water served as control. The infrared thermal imager (testo865, Germany) was utilized every 1 min to document the temperature variations in the sample.

Cytotoxicity Assay of FA-PEG-PDA

The Y79 human retinoblastoma cells, sourced from ATCC, were seeded at a density of 8×103 cells per well and cultured using DMEM medium for 24 h in 96-well plates. Subsequently, the existing medium was substituted with fresh media containing FA-PEG-PDA (without DOX) at different concentrations. Cells were then incubated for 24 or 48 h, with five

distinct concentrations established, and the medium was employed as the blank control. Subsequently, 20 μL of CCK-8 reagent was introduced into each well, allowing it to interact with viable cells for 1 h. Absorbance readings at 450 nm were acquired by submitting a microplate reader (ELX800; BioTek Instruments, Winooski, VT). Cell viability was then determined as follows:

$$(\text{Absorbances of treated cells})/(\text{Absorbances of control cells}) \times 100\%$$

In vitro Assessment of Anticancer Efficacy

Y79 cells were seeded at a density of 8×103 cells per well and incubated with DMEM medium for 24 h at 37 °C in a 5% CO_2 atmosphere. The experimental groups included laser-only, control, DOX-only, FA-PEG-PDA-DOX, and FA-PEG-PDA-DOX + laser. FA-PEG-PDA-DOX + Laser group underwent NIR laser irradiation (808 nm) for 5 min at 1 W/cm2, and cell viability was assessed using the CCK-8 assay.

In vitro Evaluation of Intracellular Uptake and Targeting Efficiency

Y79 cells underwent treatment with DIO and DAPI for 15 min to stain the cell membranes and nuclei. FA-PEG-PDA-DOX nanoparticles were incubated with DIL for 15 min for labeling purposes. Y79 cells were cultured for 4 h with different experimental groups, including laser, control, DOX, FA-PEG-PDA-DOX, FA-PEG-PDA-DOX+FA group and FA-PEG-PDA-DOX+laser. In the FA-PEG-PDA-DOX+FA group, cells were initially treated with free FA at 37 °C for 2 h, incubated with PEG-PDA-DOX NPs for an additional 4 h, examined using a confocal laser scanning microscope (CLSM FEI tecnai 12).

Quantitative Analysis of Targeting Efficiency Using Flow Cytometry

Y79 cells were cultured and subjected to various treatments, including control, DOX only, FA-PEG-PDA-DOX, PEG-PDA-DOX+FA, and FA-PEG-PDA-DOX+laser, for 2, 4, 8, and 12 h. Then, cells were washed with PBS buffer three times, exposed to 0.5 mL of pancreatic enzyme digestive fluid, followed by centrifugation at 1000 rpm for 5 min. Afterwards, they were washed, collected, and assessed using flow cytometry (Beckmann Corporation, USA).

Animals Orthotopic Model

All animal experiments were sanctioned by Henan Key Laboratory for pharmacology of Liver Diseases and Zhengzhou University Animal Ethics Committee (certificate approval number 2023-yyy-060) and conducted following the Guide for the Care and Use of Laboratory Animals. Nude mice, aged 4 weeks and weighted 18–20 g, were procured from Gempharmatech Co., Ltd. Y79 cells (1×108/mL, 2.5 μL) were injected into the vitreous of the left eyeball of nude mice. The eyes of nude mice were regularly examined under a microscope (Olympus mvx10, Japan) every week.

In vivo Fluorescence Imaging

Ten mice with RB orthotopic xenograft tumors were randomly divided into two groups (PDA-DOX, FA-PEG-PDA-DOX). We administered DiR-stained NPs dilutions (equivalent to 5 mg/kg of DOX) via their tail veins. The nude mice were anesthetized and observed using IVIS Lumina III (Perkin Elmer) at specified time points, with the mean fluorescence intensities being recorded.

In vivo Evaluation of Photothermal/Chemotherapy Effects

Following 3 weeks of tumor cell inoculation, the eyeballs of nude mice exhibited a white visible spot, about 3 mm and noticeably protruding appearance. Subsequently, nude mice bearing RB orthotopic xenograft tumors were randomly distributed into three groups (Saline control, PDA-DOX, FA-PEG-PDA-DOX+laser), each consisting of 5 mice. Each group received an NPs solution (the equivalent of 5 mg/kg of DOX) through their tail veins once every three days. The experimental groups were also subjected to near-infrared laser treatment at 808 nm (1 W/cm^2, 2 min) for tumor site irradiation once daily.

Throughout the administration period, the temperature distribution of nude mice was assessed and captured using an infrared thermal imager (testo865, Germany). The weight fluctuations and tumor growth of the mice were monitored every three days. Subsequently, the mice were euthanized, and blood, as well as major organs, were harvested and processed with nitric acid to obtain liquid solutions. Tissue sections were analysed through immunohistochemistry, which included staining for Ki67 and hematoxylin–eosin (H&E).

Statistical Analysis

Data analyses were performed by submitting the GraphPad Prism 8 software. To statistically analyze the data, Student's *t*-test was used. Significant differences are shown as $*P < 0.05$, $** P < 0.01$, $*** P < 0.001$, *#P<0.05* and *##P<0.01*. *P*-values <0.05 were considered statistically significant.

Results and Discussion

Preparation and Characterization of FA-PEG-PDA-DOX

Scheme 1A depicts the synthesis process of FA-PEG-PDA-DOX NPs. Initially, polydopamine (PDA) NPs were prepared through the oxidation-polymerization of dopamine. The average size of PDA NPs was 66.27±0.86 nm, following our previously established conditions outlined in Section (2.2. PDA synthesis). The diameter of PDA could be adjusted by manipulating the molar ratio of ammonia to dopamine. Decreasing the molar ratio or extending the reaction time gradually increases the PDA size.

The amino group of FA-PEG-NH_2 readily underwent coupling with the pyrocatechol moieties of the surface of PDA, leading to the formation of the crucial nanoparticles (FA-PEG-PDA) through Michael addition or Schiff base reaction.[31–33] In the final step, the positively charged DOX hydrochloride was assembled into FA-PEG-PDA NPs through hydrophobic interactions, π−π interactions, and electrostatic attractions on the negatively charged PDA surface. This resulted in the formation of the desired FA-PEG-PDA-DOX.

Drug loading was obtained using HPLC. Initially, a standard curve was generated by plotting the peak area A against the corresponding concentration C, as illustrated in Figures S1–S3. Subsequently, the loading content of DOX was quantified as 16.60±0.61% (w/w) for PDA-DOX and 15.38 ±0.80% (w/w) for FA-PEG-PDA- DOX, simultaneously, the EE of DOX was determined as 92.16%±1.71 (w/w) for PDA-DOX and 85.42±1.46% (w/w) for FA-PEG-PDA- DOX, using HPLC.

Polydopamine (PDA) is a promising photothermal agent and drug carrier with substantial potential in biomedical applications. Its favorable properties include a natural composition, non-toxicity, excellent biocompatibility, and high photothermal conversion efficiency (40%).[12,27,34,35]

Recent studies have affirmed that nanoparticles (NPs) with diameters ranging from 10 to 200 nm can readily penetrate the BRB. Furthermore, the immune system cannot quickly recognize and clear these NPs.[36,37] Earlier studies have indicated that positively charged NPs can be swiftly cleared from the bloodstream by the mononuclear phagocytic system.[38,39] The systemic delivery route often results in short circulation time. Additionally, lipophilic, small, and cationic molecules may bind with the melanin in RPE during systemic delivery, hindering their ability to traverse this tissue.[40,41] So, we developed the negatively charged drug delivery system (FA-PEG-PDA-DOX) (around 99nm).

The TEM images revealed that the resulting FA-PEG-PDA-DOX NPs exhibited an average diameter of less than 100 nm (Figure 1A). The hydrodynamic diameter (HD) of these NPs was determined using DLS analysis. In Figure 1B and C, it can be observed that the hydrodynamic diameters of the three types of NPs gradually increased during the preparation stages: (PDA 66.27±0.86 nm), the bonding of FA-PEG-NH_2 (FA-PEG-PDA 89.58±1.02 nm), and the loading of doxorubicin (FA-PEG-PDA-DOX 99.26±1.23 nm) (Figures S4 and S5).

As depicted in Figures 1D, S4 and S5, the alterations in zeta potential further demonstrated the functional modifications on the surface of PDA NPs. The presence of pyrocatechol groups on the surface of PDA resulted in a zeta potential of −36.6 ± 2.1 mV for PDA NPs. Following the binding of the pyrocatechol moieties on the PDA surface with the amino group of FA-PEG-NH_2, the zeta potential of FA-PEG-PDA was recorded as −27.74±2.2 mV. The reduction in zeta potential can be attributed to the formation of amide groups during this process. Upon co-assembling DOX hydrochloride with FA-PEG-PDA, the zeta potential of FA-PEG -PDA-DOX was measured as −18.11±3.1 mV. The reduction in zeta potential is attributed to the incorporation of positively

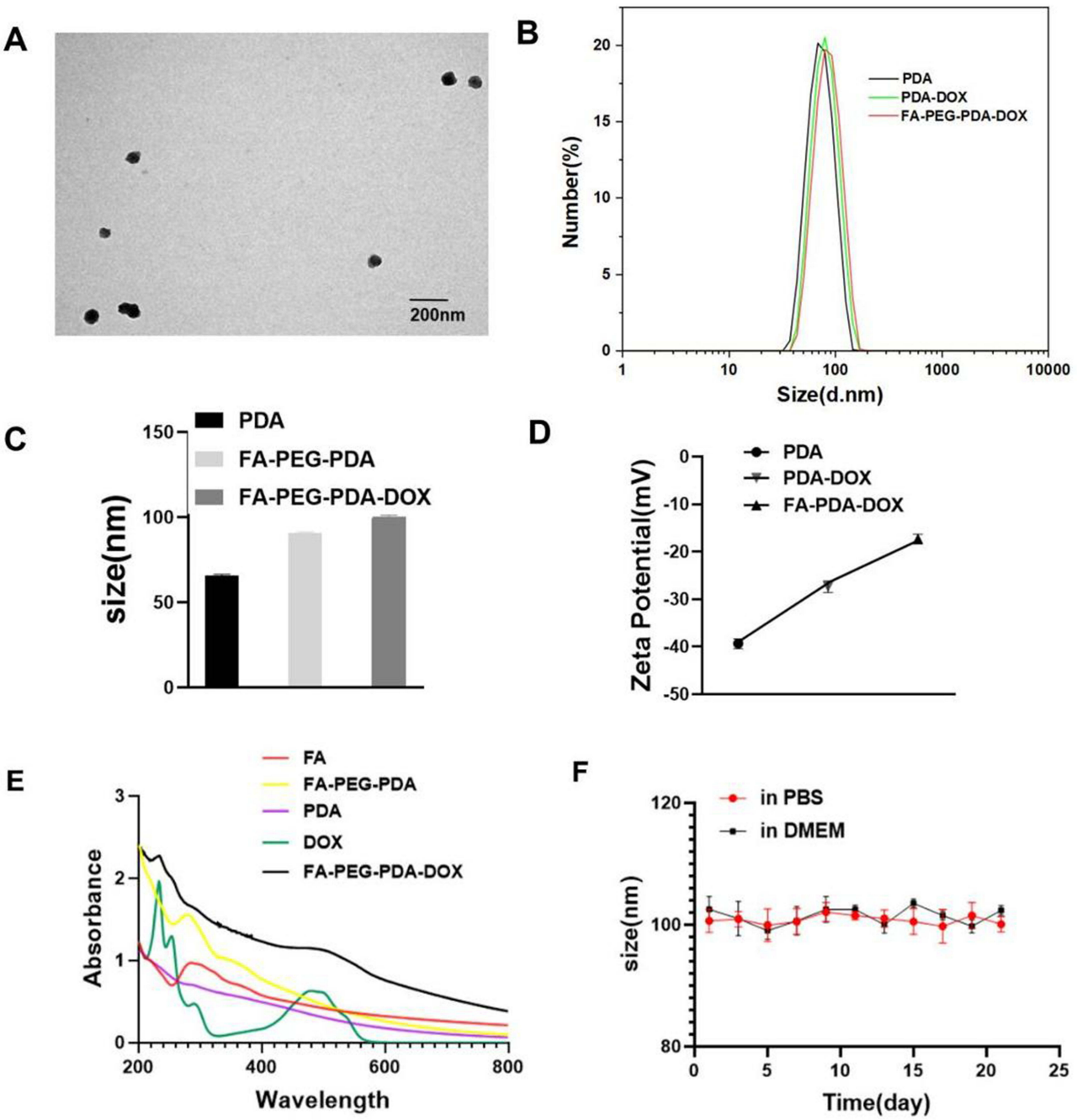

Figure 1 Characterization of NPs. (**A**) Transmission electron microscopy (TEM) image of FA-PEG-PDA-DOX. (**B**) Particle diameter distribution of PDA, FA-PEG-PDA, FA-PEG-PDA-DOX (measured by DLS). (**C**) Size analysis of three NPs. (**D**) Zeta potentials of PDA, FA-PEG-PDA, FA-PEG-PDA-DOX. (**E**) UV-vis absorption spectra of PDA, FA, DOX, A-PEG-PDA, FA-PEG-PDA-DOX (**F**) Hydrodynamic diameter profile of FA-PEG-PDA-DOX in PBS or 1640 medium for 2 weeks.

charged DOX hydrochloride. The observed alterations in both zeta potential and diameter of the NPs reflected the successful preparation of FA-PEG-PDA and the loading of doxorubicin.

The provided information aligns with the results obtained from UV-vis absorption spectra. In Figure 1E, it can be observed that there was no absorption peak at ~280 nm in UV-vis spectra of PDA. UV-vis spectra of FA-PEG-PDA displayed an augmented absorption at ~280 nm, with the peak attributed to FA. This peak indicated the successful binding of FA-PEG-NH_2 with PDA. In the UV-vis spectra of FA-PEG-PDA-DOX NPs, noticeable absorption peaks were observed at ~220 and ~480 nm. These peaks were attributed to DOX, signifying the successful loading of DOX.

Subsequently, the stability of FA-PEG-PDA-DOX NPs was evaluated (Figure 1F). The NPs maintained excellent dispersity in the tested solutions and exhibited no signs of precipitation. Their diameters remained consistent over three weeks. At various pH values, we examined the release of DOX from FA-PEG-PDA-DOX in PBS. The release of DOX was evaluated using HPLC method.

Nanoplatforms are usually translocated to lysosomes in acidic environment after receptor-mediated uptake, obtaining a lower pH-response setting.[28,42] Therefore, we mimicked lysosomal conditions by using solutions at pH 5.0 and 7.4.[28,42] As depicted in Figure 2A, the release of DOX was faster in acidic conditions than in neutral conditions. This should be attributed to the degradation of PDA in acidic systems. OH groups on surface of PDA is tended to protonate in acidic environments, which led to an elevate in the positive charge, destabilized the binding between the drug and the carrier, and finally resulted in the release of the drug from the nanosystem. The release of DOX gradually increased when FA-PEG-PDA-DOX was incubated in PBS at pH 5.0. The cumulative release of DOX from the FA-PEG-PDA-DOX NPs reached approximately 57.8% within 8 h. Under the conditions of pH 5.0 and 808 nm laser irradiation, the release of DOX increased to as high as 73.4%. In neutral conditions with a pH of 7.4, the cumulative release of DOX from the FA-PEG-PDA- DOX NPs were 16.8% within 8 h. To verify that laser irradiation promoted drug release, Ling-Xiao Zhao et al elevated the temperature of GFR dispersion up to 65 ◦C by irradiation, examined drug release under different temperature conditions.[30] Inspired by the work of the Ling-Xiao Zhao group, we also examined the drug release at 37◦C and 45 ◦C. Our data revealed that temperature elevation promoted DOX release from FA-PEG-PDA-DOX NPs; moreover, when the temperature was 45 ◦C (irradiation could elevate the temperature of FA-PEG-PDA-DOX NPs dispersion up to 45 ◦C), the release profiles was similar to that of the irradiation group (Figure 2A). These data indicated that laser

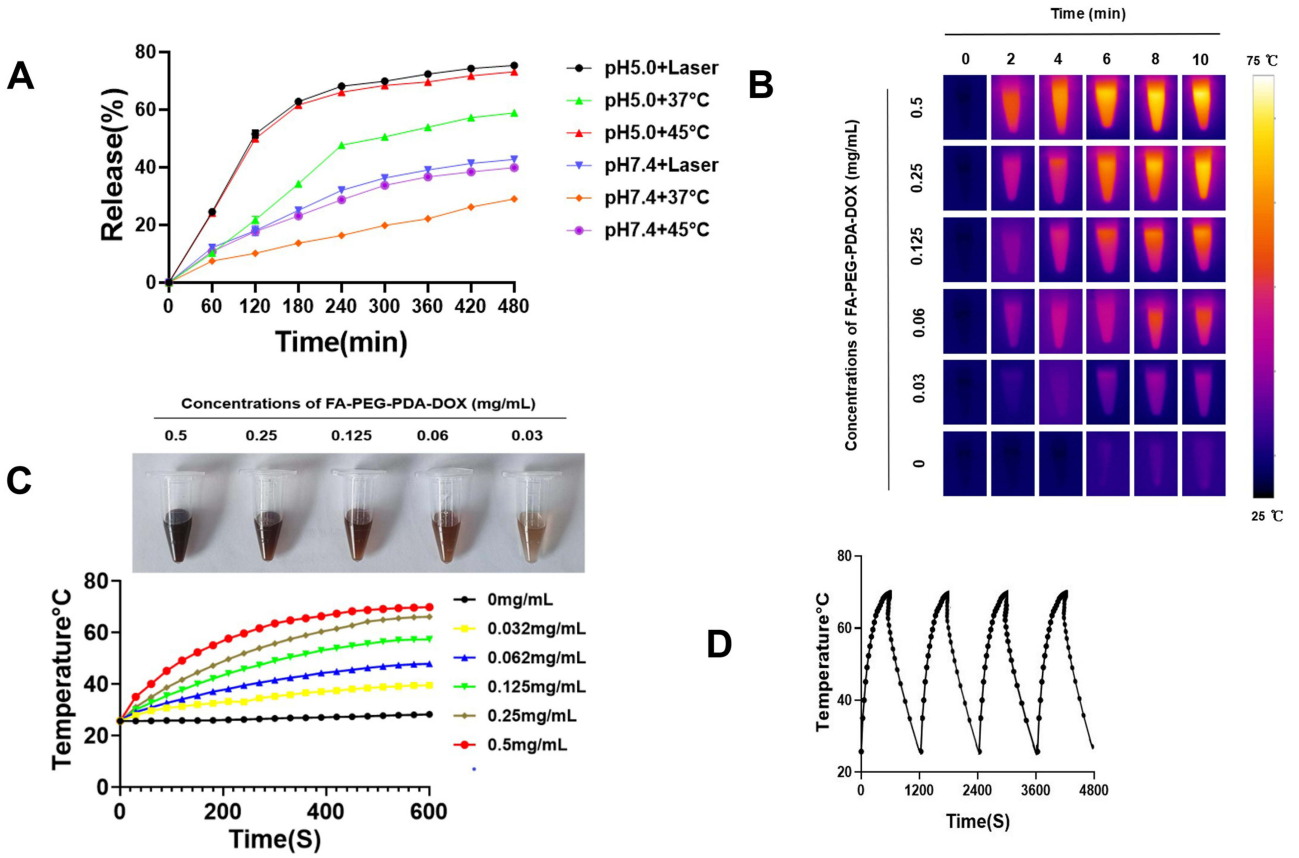

Figure 2 Characterization of NPs. (**A**) Drug release of FA-PEG-PDA-DOX and FA-PEG-PDA-DOX +Laser group at different pH conditions (pH 5.0 or 7.4). (**B**) Infrared thermal images of FA-PEG-PDA-DOX. (**C**) Concentration-dependent photothermal heating curves of FA-PEG-PDA-DOX. (**D**) Heating curve of the photothermal stability test (four laser on/off cycles).

irradiation may improve DOX release by breaking the noncovalent forces of π-π stacking between DOX and PDA through temperature elevation.[43,44]

A thermal imaging camera monitored the photothermal conversion during NIR light irradiation at 808 nm. The infrared thermal images (Figure 2B) and time-temperature curves (Figure 2C) exhibited the following trends: the temperature increased with the rising concentration (0.03, 0.06, 0.125, 0.25, and 0.5 mg/mL) and irradiation power densities at 1 W/cm^2. However, the saline did not exhibit any temperature change. This observation indicated that FA-PEG-PDA-DOX NPs possessed excellent photothermal properties. This behavior is attributed to the ability of the PDA motif to convert light energy into heat (Figure S6).

As depicted in Figure 2C, the temperature of the NPs solution rapidly reached 42 °C within two min of exposure. Notably, the concentration of the NPs was 0.5 mg/mL, which is only one-fifth of that reported in the literature for achieving a similar photothermal conversion effect.[15] This temperature point, reaching 42 °C, is crucial for cell apoptosis. Moreover, compared to normal cells, tumour cells are more susceptible to thermal damage due to poor heat dissipation, a characteristic often attributed to vascular deficiencies.[15] Therefore, it is implied that FA-PEG-PDA-DOX has the potential for effective photothermal conversion.

Furthermore, after four laser on/off (808 nm, 1W, 10 min) cycles, no significant differences in temperature were observed, indicating that FA-PEG-PDA-DOX NPs maintained excellent photothermal stability (Figure 2D).

Assessment of in vitro Cytotoxicity for FA-PEG-PDA and Synergistic Antitumor Efficacy of FA-PEG-PDA-DOX in Photothermal/Chemotherapy

The intrinsic toxicity of FA-PEG-PDA was assessed after 48 h using the cell counting kit 8 (CCK-8) assay. The results indicate that the viability of treated cells remained above 90%, even at a high concentration of 5 mg/mL. Biochemical assays of viability were further confirmed through 0.4% Trypan blue staining for dead cells (Figure 3A–C). These findings confirm the biosafety of FA-PEG-PDA as a drug carrier.

The antitumor efficacy of free DOX, PDA-DOX, FA-PEG-PDA-DOX, and FA-PEG-PDA-DOX+laser against Y79 cells was evaluated through the CCK-8 assay after 48 h of treatment. The half-maximal inhibitory concentration (IC_{50}) of the DOX group, the PDA-DOX group, the FA-PEG-PDA-DOX group, and the FA-PEG-PDA-DOX+laser group were measured as 6.68 ± 0.03, 3.88 ± 0.12, 3.25 ± 0.1, and 2.89 ± 0.24 μg/mL (equivalent of doxorubicin), respectively. Compared to the DOX group, the PDA-DOX group exhibited stronger tumor inhibition. This effect may be attributed to the enhanced permeability and retention (EPR) associated with nanomedicine.[23,24]

The FA-PEG-PDA-DOX group exhibited lower cell viability than the PDA-DOX group, demonstrating the targeted recognition of FA-PEG-PDA-DOX to FR-overexpressing Y79 cells. The lowest cell viability was observed in the FA-PEG-PDA-DOX+laser group (Figures 3D and S7). These results indicate the necessity of synergistic antitumor effects through photothermal and chemotherapy.

In vitro Analysis of Cellular Uptake and Targeting Efficiency

To confirm the ability of FA-PEG-PDA-DOX to target Y79 cell that overexpress the FA receptor, we compared the cellular uptake of free DOX (group 1), FA-PEG-PDA-DOX (group 2), and FA-PEG-PDA-DOX + antagonized folate receptors (group 3) through confocal laser scanning microscopy (CLSM) imaging. The cytomembranes and nuclei of Y79 cells were labeled green and blue, respectively. Fluorescein-labeled nanoparticles showed red color and entered the cytoplasm via cytomembranes of Y79 cells (Figure 3E). Upon treating Y79 cells with free DOX group 1, we observed some red fluorescence signals. However, when Y79 cells were incubated with group 2, the red fluorescence signal became much stronger than in group 1. This observation confirms the specific targeting capability of FA-PEG-PDA-DOX to FR-overexpressing Y79 cells. Therefore, the FA-PEG-PDA-DOX group exhibited excellent targeting performance toward Y79 cells. However, the red fluorescence signal almost disappeared in the Y79 cells of group 3, indicating fewer FRs available in the cells due to the antagonized folate receptors. This occurred due to the competitive binding with free FA. Furthermore, FA-PEG-PDA-DOX+ laser group 3 displayed a stronger red fluorescence signal than the FA-PEG-PDA-DOX group (Figure 3E). This suggests that photothermal conversion enhanced the endocytosis behavior at the intracellular level. This is consistent with previous reports.[45,46]

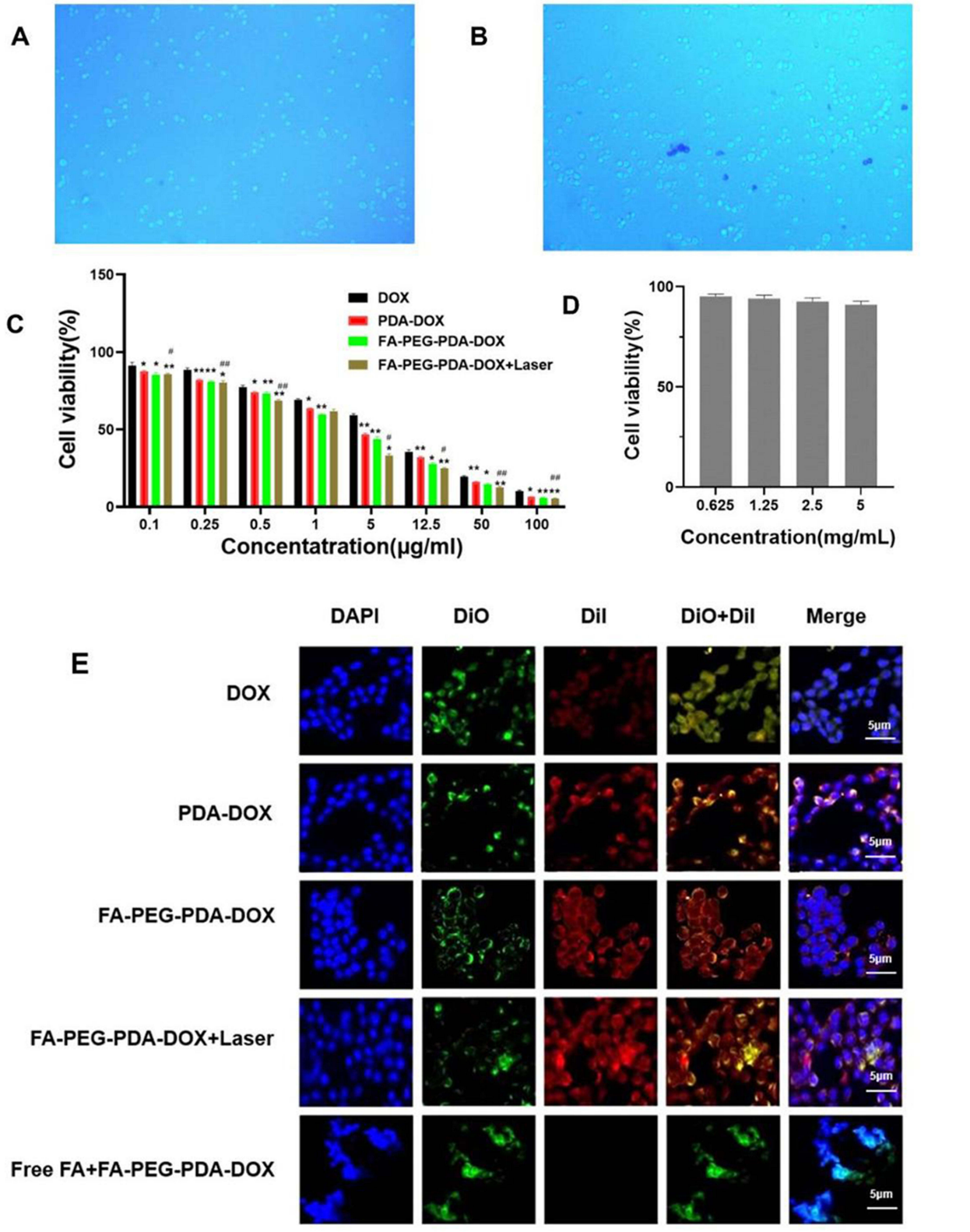

Figure 3 Cytotoxicity of FA-PEG-PDA carrier and antitumor efficacy of FA-PEG-PDA-DOX +laser in vitro. (**A**) Microscopy images of the Y79 cells with FA-PEG-PDA (5 mg/mL) incubation for 24 h and (**B**) 48 h. 0.4% trypan blue staining for dead cells. (**C**)Cytotoxicity of FA-PEG- PDA treatment (48h). (**D**) In vitro antitumor efficacy of the free DOX, PDA-DOX, FA-PEG-PDA-DOX and FA-PEG-PDA-DOX+laser. (**E**) Intracellular uptake of FA-PEG-PDA-DOX in Y79 in tumor cell lines. (Compared with DOX group $^{*}p$ <0.05, $^{**}p$ < 0.01, compared between FA-PEG-PDA-DOX and FA-PEG-PDA-DOX+Laser $^{\#}P<0.05$, $^{\#\#}P<0.01$).

The endocytosis rates were quantitatively analyzed at different times through flow cytometry analysis. The information further corroborated the CLSM results. Upon treating with the corresponding NPs, it was observed that the cell endocytosis of the FA-PEG-PDA-DOX+ Laser group was faster and higher than that of the FA-PEG-PDA-DOX group and DOX group (Figure 4A and B).

For DOX group, the cell endocytosis rates did not change significantly with time. There was a slight increase in fluorescence intensity at 12 h compared to the intensity at 2 h. After being treated for 2 h and 4 h, the intracellular fluorescence intensity of FA-PEG-PDA-DOX group was 1.9 and 2.0 times that of the DOX group, respectively. Therefore, FA-PEG-PDA-DOX group demonstrated an excellent targeting capacity toward Y79 cells.

Furthermore, Cell endocytosis rates of FA-PEG-PDA-DOX+Laser group were 2.9 and 3.1 times that of DOX group (Figure 4B), treated for 2 h and 4 h, respectively. Enhanced intensity can be attributed to its targeting performance and laser irradiation. Researchers have suggested combining PTT with other treatment modalities, such as chemotherapy, to enhance therapeutic effectiveness.[46] PTT was integrated with targeted therapy to achieve localised control of oncological tissues. This combined technique emerged as a promising strategy, effectively preventing damage to the surrounding healthy tissues. Furthermore, PTT can potentially enhance cytoplasmic gene delivery.[45]

When the incubation time reached 12 h, the fluorescence intensity of the FA-PEG-PDA-DOX+Laser group became 5.23 times that of the DOX group and 2.28 times that of FA-PEG-PDA-DOX group without irradiation (Figure 4A and B). These results confirmed the targeted recognition ability of FA-PEG-PDA-DOX nanoparticles and the synergistic effect of photothermal/chemotherapy. Figure 4C shows the average fluorescence intensity of each experimental group, with the FA-PEG-PDA-DOX+Laser group being the strongest, consistent with the cytotoxicity test results.

In vivo Assessment of Biodistribution, Targeting Efficiency, and Photothermal Conversion

Orthotopic mouse models were effectively established. Following the administration of various treatments, Fluorescence signal and biodistribution were detected (Figure 5A). The PDA-DOX group exhibited a peak fluorescence signal at 2 h, primarily observed in the internal organs and the tumor sites within the eyeballs. This was attributed to the accumulation of PDA-DOX in tumors through the EPR effect.

The fluorescent signal retained visible intensity at the tumor site for 48 h (Figure 5B). However, in the FA-PEG-PDA-DOX+Laser group, the fluorescent signal of the tumor site in the eyeballs was significantly higher than in the PDA-DOX group at every time point. This further confirmed the targeting efficiency of the FA-PEG-PDA-DOX+ laser group. This finding aligned well with the results of cell uptake in vitro. For instance, at 12 h after injection, the fluorescence intensity at tumor sites in the eyeball was more than twice as strong as that of the PDA-DOX group (Figure 5B and C).

The fluorescent signal persisted for 120 h at the tumor site within the eyeballs. This implies a significant increase in residence time, 2.5 times that of the PDA-DOX group. Therefore, we deduced that the PEGylated nanoparticles significantly prolonged the retention time in vivo (Figure 5B and C). This is in agreement with in agreement with report.[47]

Major organs and tumor tissue were subsequently removed for ex vivo analysis (Figure 5D and E). The fluorescence signals was stronger in the tumor tissue of the FA-PEG-PDA-DOX+Laser group compared to the PDA-DOX group. The fluorescent signal intensity observed at tumor sites in the eyeball was much higher than that observed in the viscera. Additionally, only the lungs showed significant fluorescence signals, and there was no obvious distribution in other organs in the FA-PEG-PDA-DOX +laser group. These effects are attributed to the targeted recognition of FA ligands, promoting superior accumulation. These results suggested that FA-PEG-PDA-DOX achieved effective accumulation in tumor tissue while minimizing damage to major organs.

In vivo Biosafety Evaluation and Assessment of Synergistic Photothermal/Chemotherapy Effects

Mice were injected with a FA-PEG-PDA-DOX NPs solution (DOX equivalent of 5 mg/kg) via the tail vein. We examined photothermal conversion of FA-PEG-PDA-DOX NPs. And the temperature at different time points was assessed using an infrared thermal imager (testo865, Germany). Figure 6B indicated that FA-PEG-PDA-DOX NPs possessed excellent photothermal properties in vivo. Then, an 808 nm near-infrared laser (1 W/cm^2, 2 min) was employed for the therapy of tumor at mild-temperature elevated by irradiation after 2 h (Figure 6A).

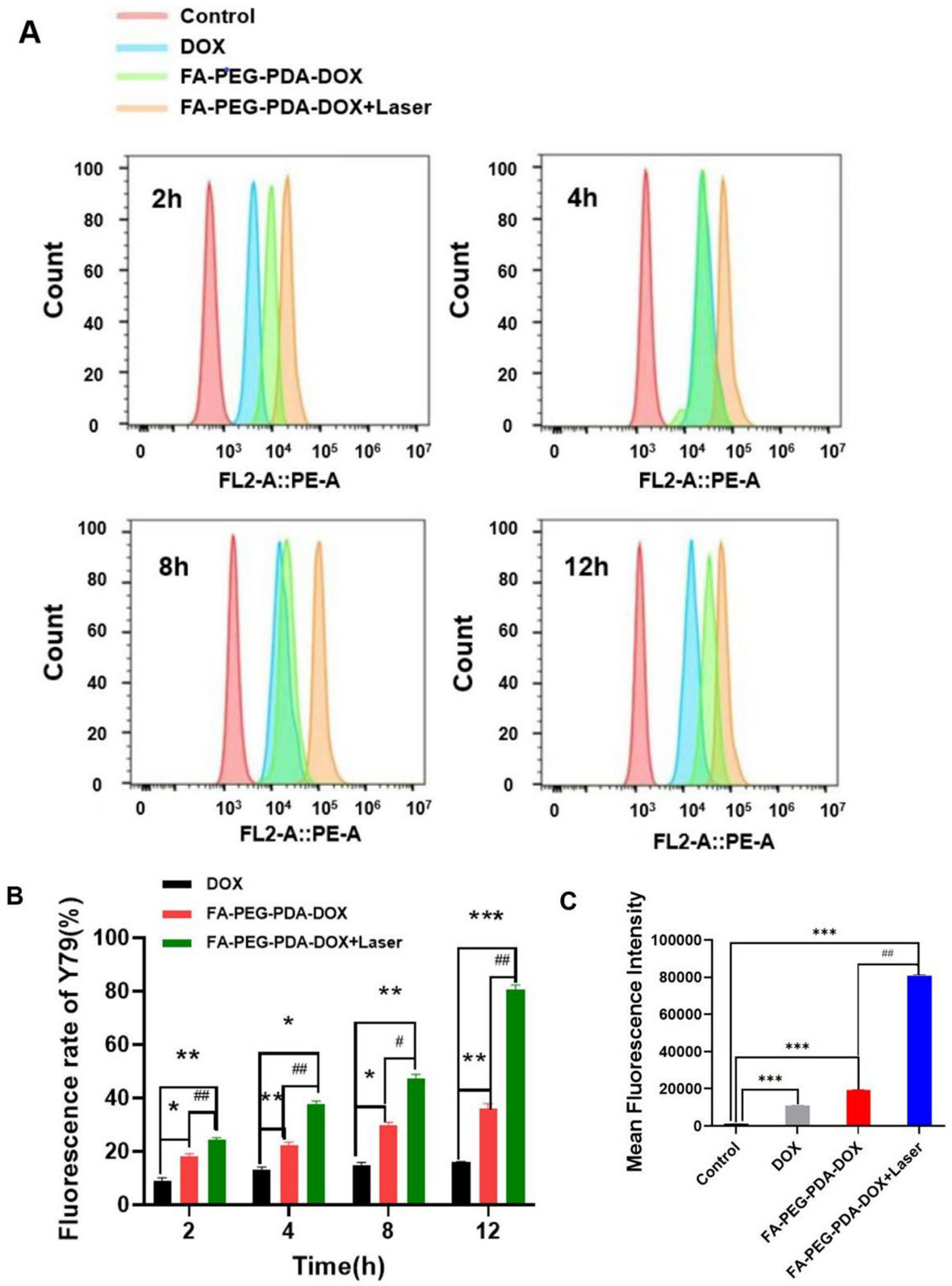

Figure 4 (**A**) intracellular uptake of quantitatively analyze by flow cytometry analysis. (**B**) intracellular uptake of quantitatively analyze by flow cytometry analysis in different groups at 2,4,8,12h.(**C**) Mean results of flow cytometric in different groups. (Compared with DOX group **p* <0.05, ***p* < 0.01, ****p* < 0.001, compared between FA-PEG-PDA-DOX and FA-PEG-PDA-DOX+laser $^{\#}P<0.05$, $^{\#\#}P<0.01$).

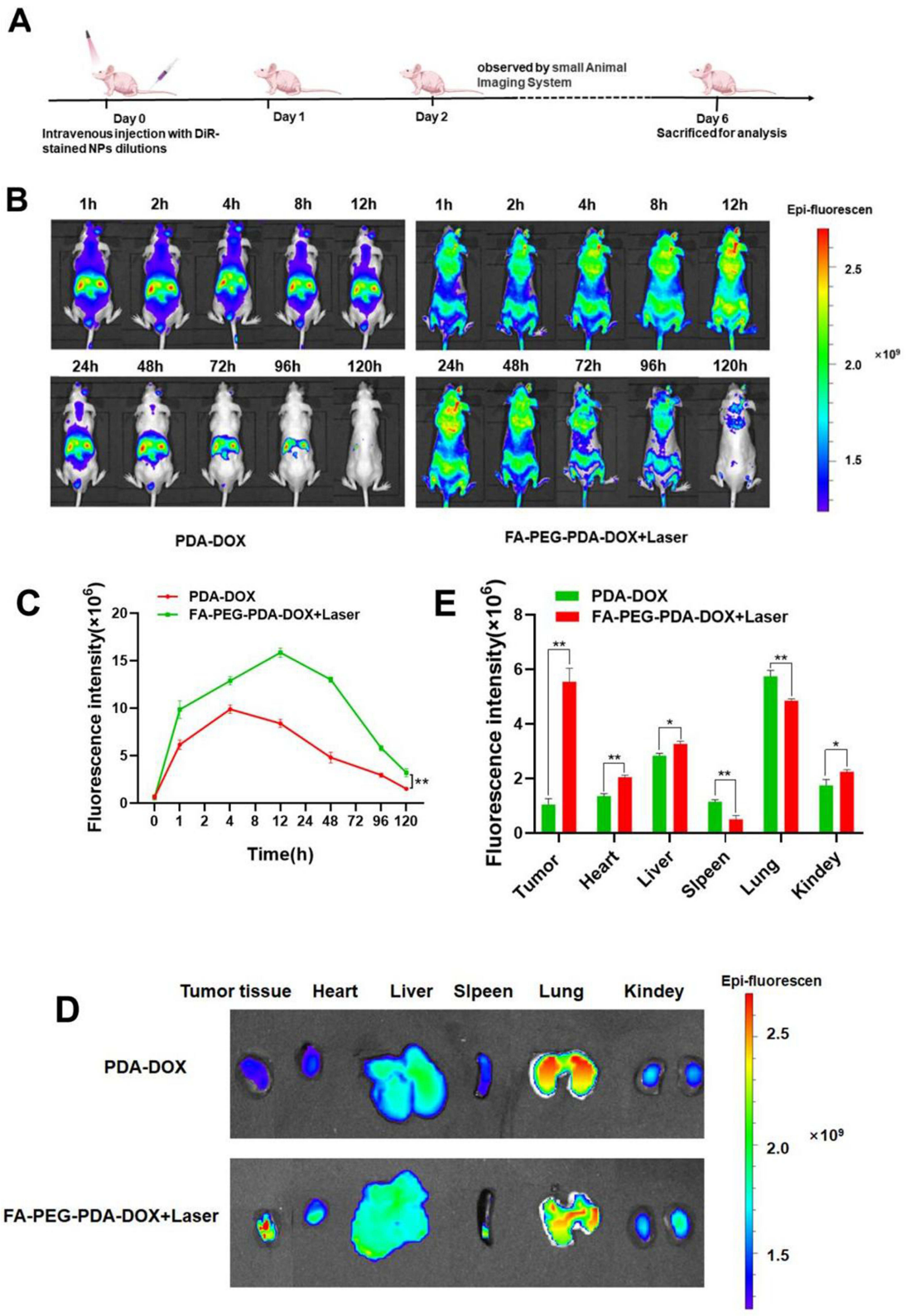

Figure 5 Fluorescence imaging and biodistribution. (**A**) Sketch map of mouse model establishment and treatment process. (**B**) fluorescence imaging of the PDA-DOX group and FA-PEG-PDA-DOX+laser group. (**C**)Quantitatively analyze of fluorescence intensity (**p < 0.01). (**D**)Biodistribution of different DiR-labeled nanoparticles in major organs and tumors. (**E**)Quantitative fluorescence in major organs and tumor tissue (*p <0.05, **p < 0.01).

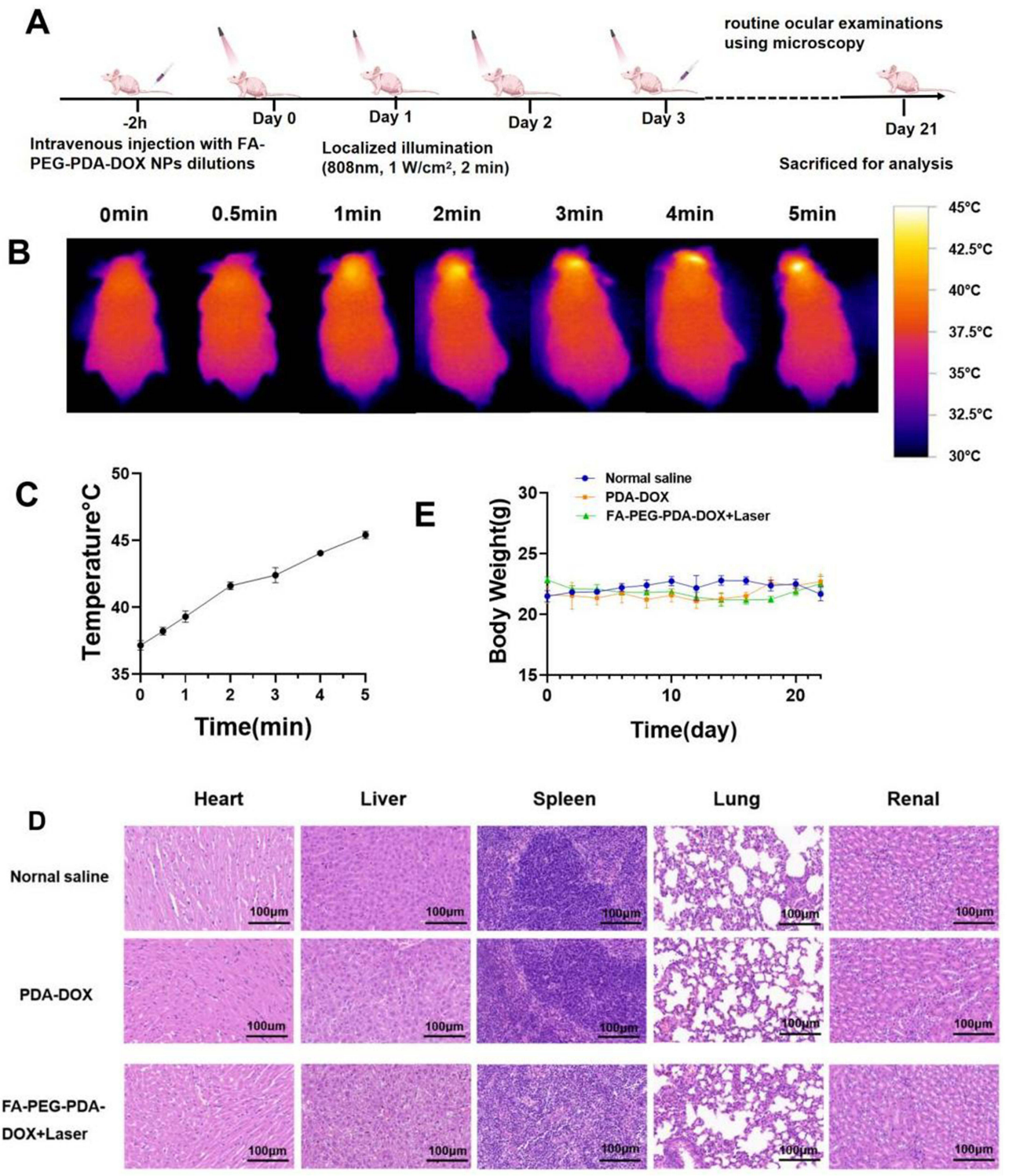

Figure 6 Biosafety and the synergistic effect of photothermal/chemotherapy in vivo. (**A**) Sketch map of in vivo treatment process. (**B**) Photothermal conversion effect in vivo. (**C**) Quantitatively analyze of photothermal conversion effect. (**D**) HE staining of essential organs. (**E**) Body weight variation of mice during treatment.

The temperature at the tumor site quickly exceeded 42 °C within 2 min of exposure, while the rest body of mice kept room temperature (Figure 6A–C). FA-PEG-PDA-DOX NPs exhibited excellent targeting recognition to Y79 tumor tissue in vivo, thereby minimizing damage to the surrounding healthy tissues. The dual functional targeted nanosystem, with the effects of DOX and mild-temperature elevation by irradiation, resulted in precise chemo/photothermal therapy in nude mice model.

To assess the safety of FA-PEG-PDA-DOX NPs, we conducted HE staining of the heart, spleen, liver, lungs, and kidneys from mice in different groups (Figure 6D). Additionally, we analyzed biochemical indexes related to liver and kidney function, including Creatinine (CREA-S), Blood Urea Nitrogen (UREA), *aspartate transaminase* (AST), and alanine transaminase (ALT) in the blood of mice.

There were no significant differences in body weight during the treatment of each group (Figure 6E), indicating that the survival status of mice was not significantly affected. No obvious side effects were observed in the histological evaluation and the blood indices (Figure 7A and B). FA-PEG-PDA-DOX NPs had no significant toxic or side effects on individual mice and

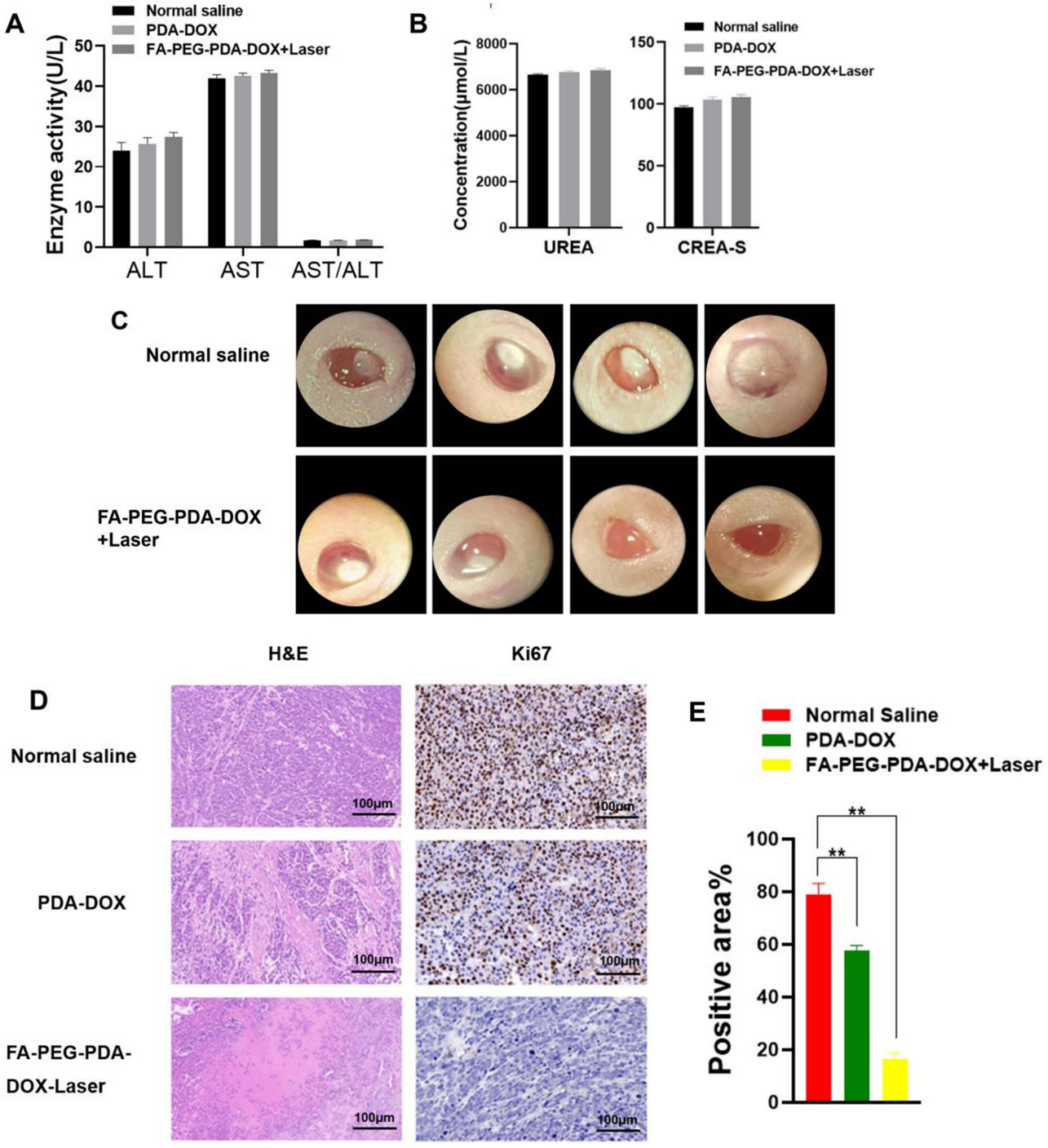

Figure 7 (**A**) Biochemical indexes analysis of liver and kidney function including AST and ALT. (**B**) Biochemical indexes analysis of liver and kidney function including CREA-S, UREA. (**C**) Photographs of the ocular surface of mice orthotopic models in different group. (**D**) HE and Ki67 staining images of tumor tissue. (**E**) Quantitatively analyze of Ki67 staining (*$p < 0.05$, **$p < 0.01$).

their organs. The histological evaluation and the blood indices revealed that FA-PEG-PDA-DOX NPs have good biosafety and high biocompatibility.

During our monitoring period, routine ocular examinations were conducted using microscopy (Motic K400, Motic Electric Group Co., Ltd). Significant tumor ablation and inhibition were observed when the mice were subjected to a combination of photothermal therapy and chemotherapy (Figure 7C). The H&E staining image of tumor sections demonstrated the synergistic effect of photothermal/chemotherapy using FA-PEG-PDA-DOX nanoparticles (Figure 7D). This resulted in more necrotic areas in the tumor, and the malignant degree of the tumor tissue was significantly reduced.

The count of tumor cells in the proliferative cycle were quantitatively analyzed by Ki67 staining image of tumor sections.[48] Ki67 is an antigen associated with proliferating cells and is indispensable for cell proliferation. Clinically, Ki67 is mainly used to label cells in the proliferative cycle.[48]

IHC analysis of Ki67 was conducted. The results showed that count of tumor cells expressing Ki67 in the photothermal/chemotherapy group (17.2%) was decreased by 61.6% compared to that of the saline control group (78.8%) (Figure 7D and E). Thus, When the mice were subjected to a combination of photothermal therapy and chemotherapy, significant tumor ablation and inhibition were observed (Figure 7C–E).

Conclusion

In summary, we developed a targeting-mediated fundus drug delivery system in this investigation that achieved the synergistic antitumor performance of photothermal and chemotherapy. FA-PEG-PDA-DOX NPs demonstrated a highly effective penetration of the BRB via the systemic route in the orthotopic models. Count of tumor cells expressing Ki67 in the photothermal/chemotherapy group (17.2%) was decreased by 61.6% compared to that of the saline control group (78.8%) FA-PEG-PDA-DOX NPs achieved significant inhibition and ablation of the tumor in a mouse orthotopic model. Moreover, the FA-PEG-PDA-DOX NPs exhibited high biocompatibility and good biosafety. Our studies provide a promising strategy for preventing the development of RB.

Abbreviations

BRB, blood-retina barrier; RB, Retinoblastoma; IAC, intra-arterial chemotherapy; PTT, Photothermal therapy; NIR, near-infrared; NPs, nanoparticles; EPR, enhanced permeability and retention.

Acknowledgments

This work was supported by Henan Provincial Science and Technology Project in (No. 232102310371, 232102310058, 242102310035, 242102310387), Key scientific research project of University in Henan Province (No.23A320067) and the Project of Basic Research Fund of Henan Institute of Medical and Pharmacological Sciences (No.2023BP0109).

Disclosure

The authors report no conflicts of interest in this work.

References

1. Mudigunda SV, Pemmaraju DB, Sankaranarayanan SA, Rengan AK. Bioactive polymeric nanoparticles of moringa oleifera induced phyto-photothermal sensitization for the enhanced therapy of retinoblastoma. *Pharmaceutics*. 2023;15(2):475. doi:10.3390/pharmaceutics15020475
2. Kaewkhaw R, Rojanaporn D. Retinoblastoma: etiology, modeling, and treatment. *Cancers*. 2020;12(8):2304. doi:10.3390/cancers12082304
3. Mudigunda SV, Pemmaraju DB, Paradkar S, et al. Multifunctional polymeric nanoparticles for chemo/phototheranostics of retinoblastoma. *ACS Biomater Sci Eng*. 2021;8(1):151–160. doi:10.1021/acsbiomaterials.1c01234
4. Jain M, Rojanaporn D, Chawla B, Sundar G, Gopal L, Khetan V. Retinoblastoma in Asia. *Eye*. 2018;33(1):87–96. doi:10.1038/s41433-018-0244-7
5. Jabbour P, Chalouhi N, Tjoumakaris S, et al. Pearls and pitfalls of intraarterial chemotherapy for retinoblastoma. *J Neurosurg Pediatr*. 2012;10 (3):175–181. doi:10.3171/2012.5.Peds1277
6. Zanaty M, Barros G, Chalouhi N, et al. Update on intra-arterial chemotherapy for retinoblastoma. *Sci World J*. 2014;2014:1–6. doi:10.1155/2014/869604
7. Arunkumar P, Raju B, Vasantharaja R, et al. Near infra-red laser mediated photothermal and antitumor efficacy of doxorubicin conjugated gold nanorods with reduced cardiotoxicity in Swiss albino mice. *Nanomed Nanotechnol Biol Med*. 2015;11(6):1435–1444. doi:10.1016/j.nano.2015.03.012
8. Liu D, Dai X, Zhang W, et al. Liquid exfoliation of ultrasmall zirconium carbide nanodots as a noninflammatory photothermal agent in the treatment of glioma. *Biomaterials*. 2023;292:121917. doi:10.1016/j.biomaterials.2022.121917

9. Lv R, Raab M, Wang Y, Tian J, Lin J, Prasad PN. Nanochemistry advancing photon conversion in rare-earth nanostructures for theranostics. *Coord Chem Rev*. 2022;460. doi:10.1016/j.ccr.2022.214486
10. Wang W, Zhang X, Ni X, et al. Semiconducting polymer nanoparticles for NIR-II fluorescence imaging-guided photothermal/thermodynamic combination therapy. *Biomater Sci*. 2022;10(3):846–853. doi:10.1039/d1bm01646f
11. Guo R, Tian Y, Wang Y, Yang W. Near-infrared laser-triggered nitric oxide nanogenerators for the reversal of multidrug resistance in cancer. *Adv Funct Mater*. 2017;27(13). doi:10.1002/adfm.201606398
12. Men X, Yuan Z. Polymer dots for precision photothermal therapy of brain tumors in the second near-infrared window: a mini-review. *ACS Appl Polymer Mater*. 2020;2(10):4319–4330. doi:10.1021/acsapm.0c00715
13. Wang Z, Li S, Zhang M, et al. Laser-triggered small interfering RNA releasing gold nanoshells against heat shock protein for sensitized photothermal therapy. *Adv Sci*. 2016;4(2). doi:10.1002/advs.201600327
14. Yang L, Hou X, Zhang Y, et al. NIR-activated self-sensitized polymeric micelles for enhanced cancer chemo-photothermal therapy. *J Control Release*. 2021;339:114–129. doi:10.1016/j.jconrel.2021.09.017
15. Li M, Bian X, Chen X, et al. Multifunctional liposome for photoacoustic/ultrasound imaging-guided chemo/photothermal retinoblastoma therapy. *Drug Delivery*. 2022;29(1):519–533. doi:10.1080/10717544.2022.2032876
16. Zheng W, Li X, Zou H, et al. Dual-target multifunctional superparamagnetic cationic nanoliposomes for multimodal imaging-guided synergistic photothermal/photodynamic therapy of retinoblastoma. *Int j Nanomed*. 2022;17:3217–3237. doi:10.2147/ijn.S364264
17. Wu M, Xiong H, Zou H, et al. A laser-activated multifunctional targeted nanoagent for imaging and gene therapy in a mouse xenograft model with retinoblastoma Y79 cells. *Acta Biomater*. 2018;70:211–226. doi:10.1016/j.actbio.2018.02.006
18. Liu Y, Han Y, Chen S, Liu J, Wang D, Huang Y. Liposome-based multifunctional nanoplatform as effective therapeutics for the treatment of retinoblastoma. *Acta Pharmaceutica Sinica B*. 2022;12(6):2731–2739. doi:10.1016/j.apsb.2021.10.009
19. Delamo E, Urtti A. Current and future ophthalmic drug delivery systemsA shift to the posterior segment. *Drug Discovery Today*. 2008;13(3–4):135–143. doi:10.1016/j.drudis.2007.11.002
20. Hasler PW, Brandi bloch S, Villumsen J, Fuchs J, Lund-Andersen H, Larsen M. Safety study of 38 503 intravitreal ranibizumab injections performed mainly by physicians in training and nurses in a hospital setting. *Acta Ophthalmologica*. 2014;93(2):122–125. doi:10.1111/aos.12589
21. Li K, Li R, Zou P, et al. Glycopeptide-nanotransforrs eyedrops with enhanced permeability and retention for preventing fundus neovascularization. *Biomaterials*. 2022;281:121361. doi:10.1016/j.biomaterials.2021.121361
22. Kansara V, Paturi D, Luo S, Gaudana R, Mitra AK. Folic acid transport via high affinity carrier-mediated system in human retinoblastoma cells. *Int J Pharm*. 2008;355(1–2):210–219. doi:10.1016/j.ijpharm.2007.12.008
23. Björnmalm M, Thurecht KJ, Michael M, Scott AM, Caruso F. Bridging bio–nano science and cancer nanomedicine. *ACS Nano*. 2017;11(10):9594–9613. doi:10.1021/acsnano.7b04855
24. Kalyane D, Raval N, Maheshwari R, Tambe V, Kalia K, Tekade RK. Employment of enhanced permeability and retention effect (EPR): nanoparticle-based precision tools for targeting of therapeutic and diagnostic agent in cancer. *Mater Sci Eng C*. 2019;98:1252–1276. doi:10.1016/j.msec.2019.01.066
25. Li X, Garamus VM, Li N, et al. Preparation and characterization of a pH-responsive mesoporous silica nanoparticle dual-modified with biopolymers. *Colloids Surf. A*. 2018;548:61–69. doi:10.1016/j.colsurfa.2018.03.047
26. Yan S, Huang Q, Chen J, et al. Tumor-targeting photodynamic therapy based on folate-modified polydopamine nanoparticles. *Int j Nanomed*. 2019;14:6799–6812. doi:10.2147/ijn.S216194
27. Liu Y, Ai K, Liu J, Deng M, He Y, Lu L. Dopamine-melanin colloidal nanospheres: an efficient near-infrared photothermal therapeutic agent for in vivo cancer therapy. *Adv Mater*. 2012;25(9):1353–1359. doi:10.1002/adma.201204683
28. Deng Z, Tang M, Zhao L, et al. Targeted H+-triggered bubble-generating nanosystems for effective therapy in cancer cells. *Colloids Surf B*. 2017;160:207–214. doi:10.1016/j.colsurfb.2017.09.034
29. Li N, Li T, Hu C, Lei X, Zuo Y, Han H. Targeted near-infrared fluorescent turn-on nanoprobe for activatable imaging and effective phototherapy of cancer cells. *ACS Appl Mater Interfaces*. 2015;8(24):15013–15023. doi:10.1021/acsami.5b02037
30. Zhao L-X, Gong Z-Q, Zhang Q, et al. Graphdiyne nanoplatforms for photothermal-ferroptosis combination therapy against glioblastoma. *J Control Release*. 2023;359:12–25. doi:10.1016/j.jconrel.2023.05.035
31. Duo Y, Yang M, Du Z, et al. CX-5461-loaded nucleolus-targeting nanoplatform for cancer therapy through induction of pro-death autophagy. *Acta Biomater*. 2018;79:317–330. doi:10.1016/j.actbio.2018.08.035
32. Zhang DY, Zheng Y, Zhang H, et al. Delivery of phosphorescent anticancer iridium(III) complexes by polydopamine nanoparticles for targeted combined photothermal-chemotherapy and thermal/photoacoustic/lifetime imaging. *Adv Sci*. 2018;5(10). doi:10.1002/advs.201800581
33. Cheng W, Zeng X, Chen H, et al. Versatile polydopamine platforms: synthesis and promising applications for surface modification and advanced nanomedicine. *ACS Nano*. 2019;13(8):8537–8565. doi:10.1021/acsnano.9b04436
34. Yan S, Song X, Liu Y, et al. An efficient synergistic cancer therapy by integrating cell cycle inhibitor and photosensitizer into polydopamine nanoparticles. *J Mat Chem B*. 2018;6(17):2620–2629. doi:10.1039/c8tb00076j
35. Della Vecchia NF, Luchini A, Napolitano A, et al. Tris buffer modulates polydopamine growth, aggregation, and paramagnetic properties. *Langmuir*. 2014;30(32):9811–9818. doi:10.1021/la501560z
36. Bisht R, Mandal A, Jaiswal JK, Rupenthal ID. Nanocarrier mediated retinal drug delivery: overcoming ocular barriers to treat posterior eye diseases. *WIREs Nanomed Nanobiotechnol*. 2017;10(2). doi:10.1002/wnan.1473
37. Kievit FM, Zhang M. Cancer nanotheranostics: improving imaging and therapy by targeted delivery across biological barriers. *Adv Mater*. 2011;23(36):H217–47. doi:10.1002/adma.201102313
38. Guasch A, Deen WM, Myers BD. Charge selectivity of the glomerular filtration barrier in healthy and nephrotic humans. *J Clin Investig*. 1993;92(5):2274–2282. doi:10.1172/jci116831
39. Gullotti E, Yeo Y. Extracellularly activated nanocarriers: a new paradigm of tumor targeted drug delivery. *Mol Pharmaceut*. 2009;6(4):1041–1051. doi:10.1021/mp900090z
40. Edelhauser HF, Rowe-Rendleman CL, Robinson MR, et al. Ophthalmic drug delivery systems for the treatment of retinal diseases: basic research to clinical applications. *Investigat Opthalmol Vis Sci*. 2010;51(11). doi:10.1167/iovs.10-5392

41. Pitka¨Nen L, Ranta V-P, Moilanen H, Urtti A. Permeability of retinal pigment epithelium: effects of permeant molecular weight and lipophilicity. *Investigat Opthalmol Vis Sci*. 2005;46(2). doi:10.1167/iovs.04-1051
42. Zhang Y, Fu X, Jia J, et al. Glioblastoma therapy using codelivery of cisplatin and glutathione peroxidase targeting siRNA from iron oxide nanoparticles. *ACS Appl Mater Interfaces*. 2020;12(39):43408–43421. doi:10.1021/acsami.0c12042
43. Yuan Z, Lin C, He Y, et al. Near-infrared light-triggered nitric-oxide-enhanced photodynamic therapy and low-temperature photothermal therapy for biofilm elimination. *ACS Nano*. 2020;14(3):3546–3562. doi:10.1021/acsnano.9b09871
44. Gao G, Jiang Y-W, Jia H-R, Wu F-G. Near-infrared light-controllable on-demand antibiotics release using thermo-sensitive hydrogel-based drug reservoir for combating bacterial infection. *Biomaterials*. 2019;188:83–95. doi:10.1016/j.biomaterials.2018.09.045
45. Kim J, Kim J, Jeong C, Kim WJ. Synergistic nanomedicine by combined gene and photothermal therapy. *Adv Drug Delivery Rev*. 2016;98:99–112. doi:10.1016/j.addr.2015.12.018
46. Gao G, Jiang YW, Sun W, et al. Molecular targeting-mediated mild-temperature photothermal therapy with a smart albumin-based nanodrug. *Small*. 2019;15(33). doi:10.1002/smll.201900501
47. Veronese FM, Pasut G. PEGylation, successful approach to drug delivery. *Drug Discovery Today*. 2005;10(21):1451–1458. doi:10.1016/s1359-6446(05)03575-0
48. Xu H, Xiao L, Chen Y, et al. Effect of CDK7 inhibitor on MYCN-amplified retinoblastoma. *Bioch et Biophys Acta*. 2023;1866(3):194964. doi:10.1016/j.bbagrm.2023.194964